A family of high-flow Roots blower profiles based on non-circular gears and the coin rotation paradox

A preprint

Robert W. Horst
Department of Electrical and Computer Engineering
University of Illinois at Urbana-Champaign
bhorst@illinois.edu

July 15, 2025

Abstract

Roots blowers are positive displacement pumps that trap the air in pockets of counter-rotating rotors. This paper describes and analyzes a new family of high-flow Roots blower profiles which are shown to have flow rates as high as 3.9 times the flow rate of those based on epicycloid/hypocycloid arcs. The profiles can be used to build either straight-lobe or helical rotors. For a given airflow requirement, the new profiles allow for reduced RPM and lower acoustic noise and may open up new applications for Roots blowers in consumer applications. Simplified equations for the profiles of a circle rolling around a noncircular gear are derived using the lessons from the coin rotation paradox. The equations take advantage of previous work in noncircular gear theory but advance that theory to produce an equation that produces a range of identical noncircular gears with any number of lobes. Interferences in the resulting profiles are eliminated by offsetting the profiles. The resulting profiles are more eccentric and higher flow than traditional Roots profiles. Estimates of the flow rates show that the small amount of carryover is more than overcome by the greater flow rates of the new profiles. Multiple variations of the profiles are illustrated by figures showing the meshing of rotors at different angles.

Keywords *Roots blower; noncircular gear; rotor profile; rotary lobe pump; helical rotor*

1. Introduction

Roots blowers, also known as rotary lobe blowers, are positive displacement pumps that move air by trapping the air in pockets of counter-rotating rotors. The pockets are formed by the space between the rotors and the casing. The original Roots blower used two-lobed rotors, but other rotor profiles with three or more lobes are now common. Figure 1 shows an example of a 3-lobed rotor with air entering the suction port, flowing around the outside of both rotors, and exiting from the exhaust port.

Roots blowers are used to move or compress air or gasses in a wide variety of industries but have seen little application in consumer blowers or in electronics cooling. This paper offers improvement in the flow rate of Roots blowers that may make them more suitable for those uses.

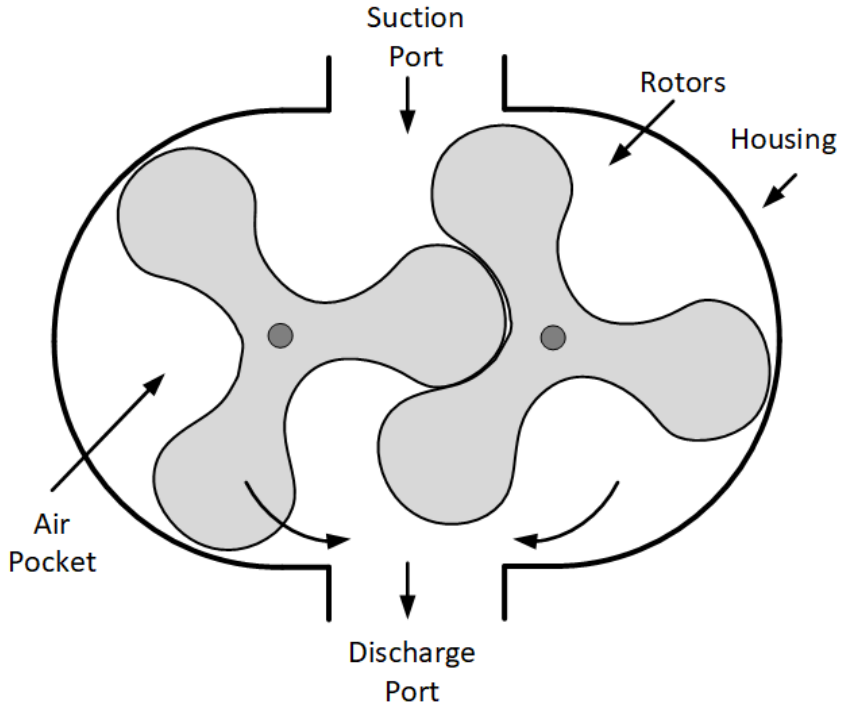

Figure 1. 3-lobe Roots blower cross section

2. Prior work in Roots blower profiles

Roots blower profiles have undergone a series of modifications and improvements since the concepts of the Roots Blower was invented and patented by the Roots brothers [1]. In 1873, the profile was modified by Palmer and Knox to form the addendum and dedendum from an epicycloid and hypocycloid, respectively [2]. This EH profile is formed by a point on the circumference of a rolling circle that rolls around the outside of the pitch circle to generate the epicycloid, and rolls around the inside of the pitch circle to generate the hypocycloid. The EH profile has been the basis for comparison to newer profiles. The 2018 paper by Wu and Tran presents the equations for EH profiles along with a CIC profile. The CIC rotor profile is comprised of a circular arc, an involute curve and a conjugated circular arc [3]. The CIC profile was also analyzed in the 1980 paper by Ucer and Celik [4].

Zauo, in a 2023 paper, proposes a novel Roots profile that consists of six curves and a sharp point [5]. The new profiles involve increasing complexity. The Zauo paper has four reference coordinate systems and two full pages of parametric equations. While this profile is an improvement over some prior profiles, the math complexity makes it a daunting task for an engineer to implement.

Several papers have suggested generation of Roots profiles by rolling a circle or ellipse outside and inside a pitch path. With a circular roller and circular pitch path, this method generates the

standard epicycloid-hypocycloid profiles introduced in 1873. Tien proposed a Roots profile based on rolling a circle around an ellipse [6].

The Roots profiles in this paper are based on rolling a circle around identical noncircular gear pitch profiles. A theory for generating these noncircular pitch curves was presented in 1998 by Tong [7]. The pitch curves can also be generated based on the noncircular gears presented by Litvin and Bair [8,9]. These papers present noncircular gears based a driven gear, with the conjugate gear determined based on the spacing and phase of the driven gear. The equation for an N-lobe driven gear is given by:

$$\rho_{1(\theta)} = \frac{a(1-\varepsilon)}{1+\varepsilon(\cos(N * \theta))} \tag{1}$$

Where ρ is the radius at each angle θ, α is the semi-major axis distance, ε is the eccentricity and N is the number of lobes. The conjugate noncircular gear equation is simply:

$$\rho_{2(\theta)} = ss - \rho_{1(\theta)} \tag{2}$$

where ss is the shaft spacing.

While Eq 1 and Eq 2 can be used for noncircular gearing, the two gears are not identical. Generating Roots profiles requires the noncircular gears to have identical pitch profiles. If Equation 1 is used for both gears, but with the second gear rotated by 90°, they mesh at the 90° rotation intervals, but do not quite mesh in between. A correction can be made, with half the correction made to each gear to make identical gears that mesh at all rotation angles. Then the equations for the radius of the identical N-lobe noncircular gears at angle θ are:

$$\begin{cases} \rho_{3(\theta)} = \dfrac{a(1-\varepsilon^2)}{1+\varepsilon(\cos(N * \theta))} + \dfrac{\Delta_\rho(\theta)}{2} \\ \rho_{4(\theta)} = \dfrac{a(1-\varepsilon^2)}{1+\varepsilon\left(\cos\left(\frac{\pi}{N}+N * \theta\right)\right)} + \dfrac{\Delta_\rho(\theta)}{2} \\ \Delta_\rho(\theta) = ss - \dfrac{a(1-\varepsilon^2)}{1+\varepsilon(\cos(N * \theta))} - \dfrac{a(1-\varepsilon^2)}{1+\varepsilon\left(\cos\left(\frac{\pi}{N}+N * \theta\right)\right)} \end{cases} \tag{3}$$

Figure 2 shows three-lobe circular gears with and without the correction to make them mesh at all pitch angles.

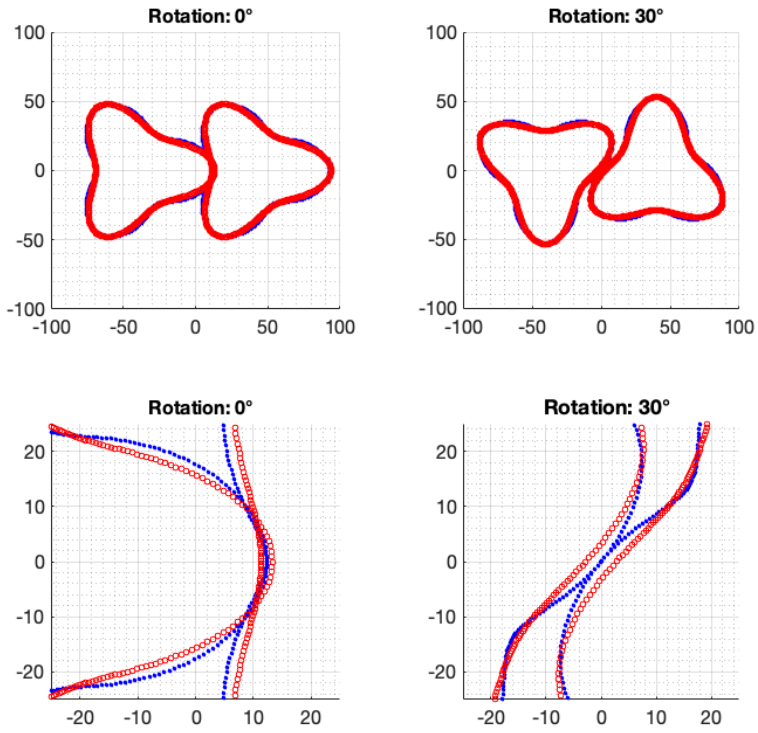

Figure 2. Full and closeup profiles of three-lobe circular gears with ε = 0.3 at two different rotation angles. The red circles show identical uncorrected profiles from Equation 1 and the blue points show the corrected profiles from Equation 3. Dimensions are in mm.

In Figure 2, at 0º rotation there is interference between the uncorrected gear profiles and at 30º, there is a gap between the uncorrected gear profiles. The corrected profiles have no interference or gaps at any rotation angle.

3. Profiles based on rolling a circle around noncircular gears

Tien et. al. proposed a Roots profile based on rolling a circle around an ellipse, but the paper does not extend the idea to more than two lobes and does not discuss corrections to make center-axis ellipses mesh at all angles [11].

The Roots blower profiles in this paper are based on rolling a circle around a noncircular gear profile. Any type of center-axis, identical gear could be used, including those proposed by Tong [10] but this paper presents only the noncircular gears based on Equation 3 above. The radius of the rolling circle, r_c, is determined by the number of lobes and the circumference of the noncircular gear.

$$r_c = \frac{\int_0^{2\pi} \rho(\theta) d\theta}{4\pi N} \tag{6}$$

The circumference of the noncircular gear is determined by converting the points to polar notation and numerically integrating the radius of the gear from 0 to 2π. The denominator is set to

allow the circle radius to fully rotate once for each addendum and once for each dedendum. With 2 lobes, the rolling distance around the noncircular gear is $8\pi r_c$ and with 3 lobes, the distance is $12\pi r_c$.

The lobes are formed by rolling on the outside of the gear for the addendum and rolling on the inside of the gears for the dedendum. The math is greatly simplified relative to other papers that derive complex parametric equations based on translation between different reference frames and determining a constant rate of curvature at transition points between addendum and dedendum.

The rolling of a circle around another shape is a form of a problem known as the coin rotation paradox [13]. When rolling a coin around one with three times the diameter, to get back to the original position, it rotates four times, not three times. This can be understood by rolling the coin along a straight belt with length three times the circumference of the small coin. When that belt is then wrapped around the large coin, it rotates one more time.

When the circle rotates on the outside of the gear for each addendum, its position in polar coordinates is the position of the center of the circle plus the rotation of the circle around its center. For the addendum of a 2-lobe rotor, the circle rotates 4 + 1 = 5 degrees for every one degree of change around the gear perimeter. For the dedendum, rolling on the inside, it rotates 4 - 1 = 3 degrees for every one degree of change around the gear perimeter. For a 3-lobe rotor, it rotates 7 times for the addendum and 5 times for the dedendum. The equations for an N-lobe rotor are simply:

Addendum

$$\begin{cases} \phi = \theta(2N+1) \\ P_x = (\sigma_3 + r_c)\cos\theta + r_c\cos\phi \\ P_y = (\sigma_3 + r_c)\sin\theta + r_c\sin\phi \end{cases} \tag{7}$$

Dedendum

$$\begin{cases} \phi = \theta(2N-1) \\ P_x = (\sigma_3 - r_c)\cos\theta - r_c\cos\phi \\ P_y = (\sigma_3 - r_c)\sin\theta - r_c\sin\phi \end{cases} \tag{8}$$

where θ is the angle from the X axis to the point (P_x and P_y) of the rotor, r_c is the radius of the rolling circle, and ϕ is the rotation angle of the circle. For the addendum, the center of the circle is the sum of the radius of the gear and the circle, while for the dedendum, the center of the circle is the gear radius minus the circle radius. The circle rotation direction is positive for the addendum and negative for the dedendum.

3.1. Interference and gaps

The rotor profiles generated by the rolling circle mesh perfectly if the noncircular gear is convex, such as when $\varepsilon = 0$ (with the gear shape a circle). However, at larger values of ε, the noncircular gear is partially concave, and if the radius of curvature of the concave portion is less than that of the circle, the resulting gear shapes interfere with each other at some rotation angles.

One way to solve the interference problem is simply to avoid the problem by restricting the solution set to less eccentric designs that avoid the interferences. This paper takes a different approach and allows more eccentric rotor shapes by offsetting the profiles to reduce the rotor radius at all angles until the interference is avoided. This reduction introduces undercutting and carryover

volume, which are normally avoided in Roots profile design. (Carryover is the term that describes air that is trapped and returned to the input or recirculated, instead of being delivered to the discharge port.) However, the approach taken here more than makes up for the carryover volume by increased airflow due to the improved area efficiency.

3.2. Offsets

To create the offset profile, at each point, the normal angle is derived as 90° from the tangent angle, then the radius at that angle is reduced by the *offset* value. Alternatively, the new profile can be derived using the Matlab *offsetCurve* function, or by using a 3D CAD tool such as the Autodesk Fusion *Offset* feature. To determine when *offset* is large enough to avoid all interferences, a simple brute-force approach has been used to measure the distance between all points of both profiles at a large number of rotation angles. For Figures 4-6 and tables 1-2, 360 rotation angles are used with 1001 points for the rotor profiles. The Matlab code to determine minimum gaps for a given offset was first written as a triple-nested loop, but each offset value took several minutes to analyze. By vectorizing the Matlab code, this time was reduced to a few seconds. The vector code was used both to find profiles with 0.1 mm minimum gaps and for 2 mm minimum gaps. The average gaps were also determined for the airflow calculations.

Figure 3 shows the construction of 2-lobe and 3-lobe rotors with 0.1 mm minimum gaps. The solid lines are the noncircular gear shapes used to generate the rotor profiles.

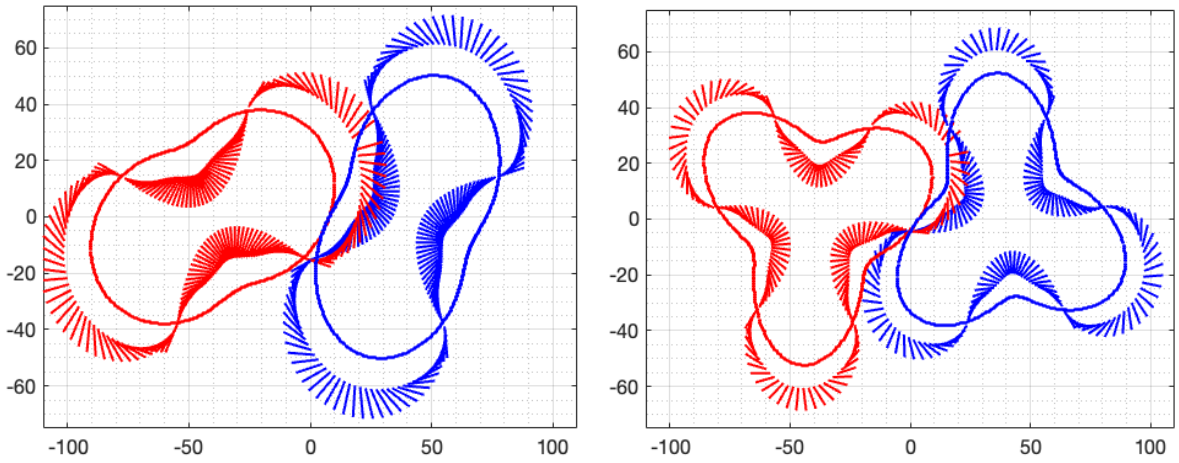

Figure 3. Derivation of Roots profiles from rolling a circle outside and inside a 2-lobe or 3-lobe noncircular gear with ε = 0.3 and 180 points. Straight lines connect the center of the rolling circle to the point on the circle defining the profile.

Figure 4 illustrates Roots profiles after applying the offsets. The illustrated shapes include offsets that avoid interference between the rotors. Before the offset is applied, the rotors would interfere with each other. The offset is adjusted until the minimum rotor-rotor gap is the desired gap, based on the manufacturing tolerances. This figure also illustrates the large difference in air pocket volume for designs with higher eccentricity.

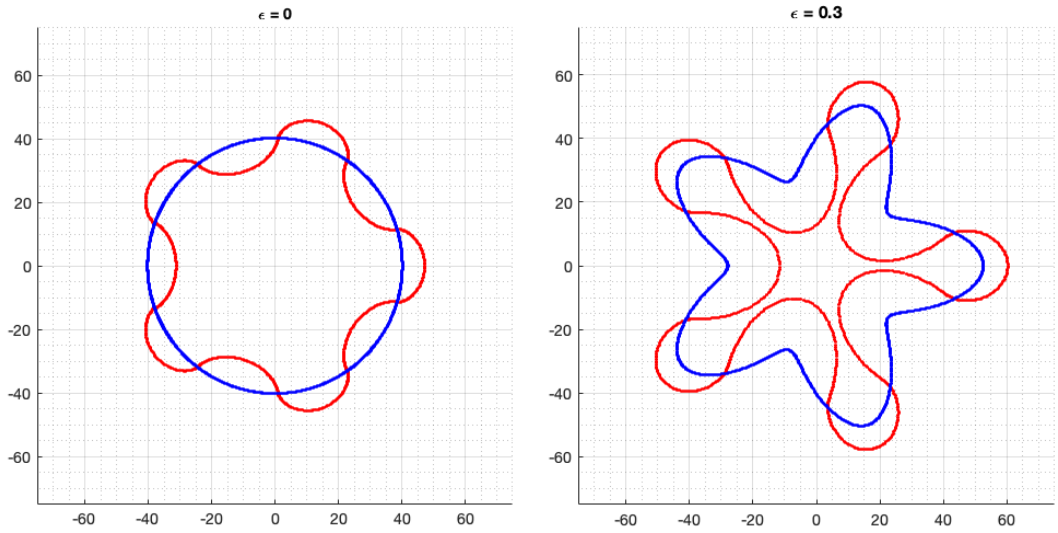

Figure 4. Five lobe rotors showing the noncircular gear in blue and the final offset rotor shape in red. The left rotor is the standard epicycloid-hypocycloid shape based on rolling a circle ($\varepsilon = 0$) around a larger circle. The right rotor is based on noncircular gears with $\varepsilon = 0.3$ and has a calculated flow rate 3.9 times greater.

Figure 5 shows graphs of the minimum inter-rotor gap (in mm) vs. rotation angle (in degrees) for several different rotor shapes. When the "noncircular" gear is in fact circular, with $\varepsilon = 0$, the minimum gap is equal to twice the offset and does not vary with rotation angle. With $\varepsilon > 0$, there are periodic peaks in the minimum gap, indicating the condition known in gear design as *undercutting*. At these angles, a pocket is formed in the gap between the rotors, and the rotor exhibits *carryover*, meaning that some air is returned to the input instead of being delivered to the output. The effect of this carryover volume is analyzed in the section on airflow estimates.

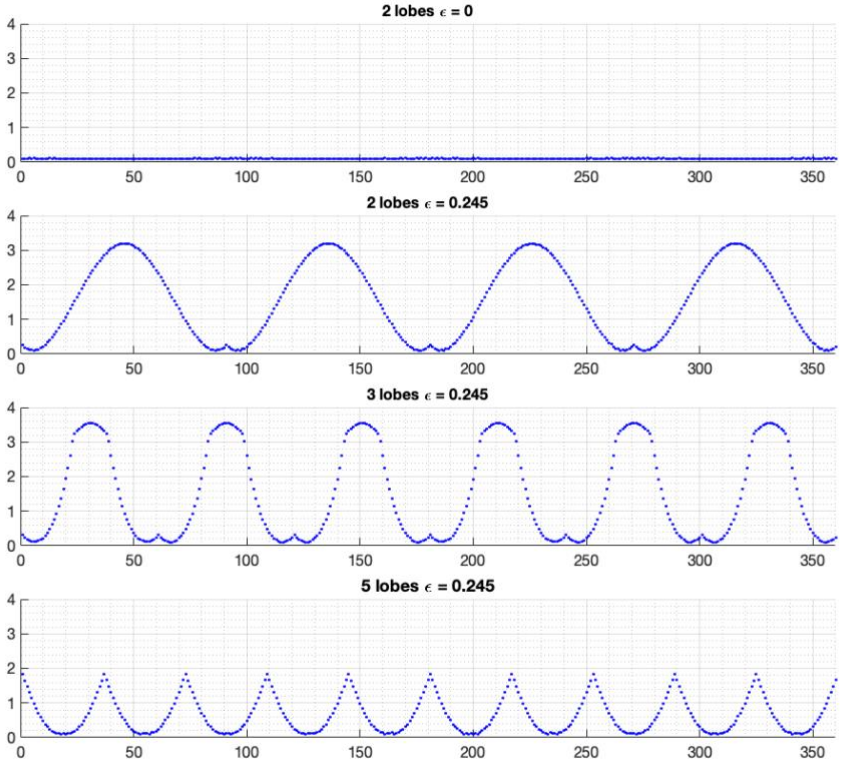

Figure 5. Minimum gap vs rotation angle for profiles with 2, 3 and 5 lobes.

4. Rotor profiles

Figure 6 shows rotor profiles for 2-5 lobes for a range of ε values. This figure also shows the noncircular gears used to derive each profile. Note that the air volume increases as ε increases, but at some point, a limit is eventually reached. For 2-lobe rotors, the minimum rotor radius decreases sharply and eventually reaches a point where it is too small for the required shaft and bearings to support the rotor. With a greater number of lobes, the lobes eventually are reduced to a size too thin to maintain their shape. Engineering constraints on the problem being addressed are used to limit the design space and allow selection of the most appropriate profile from the family of possible profiles.

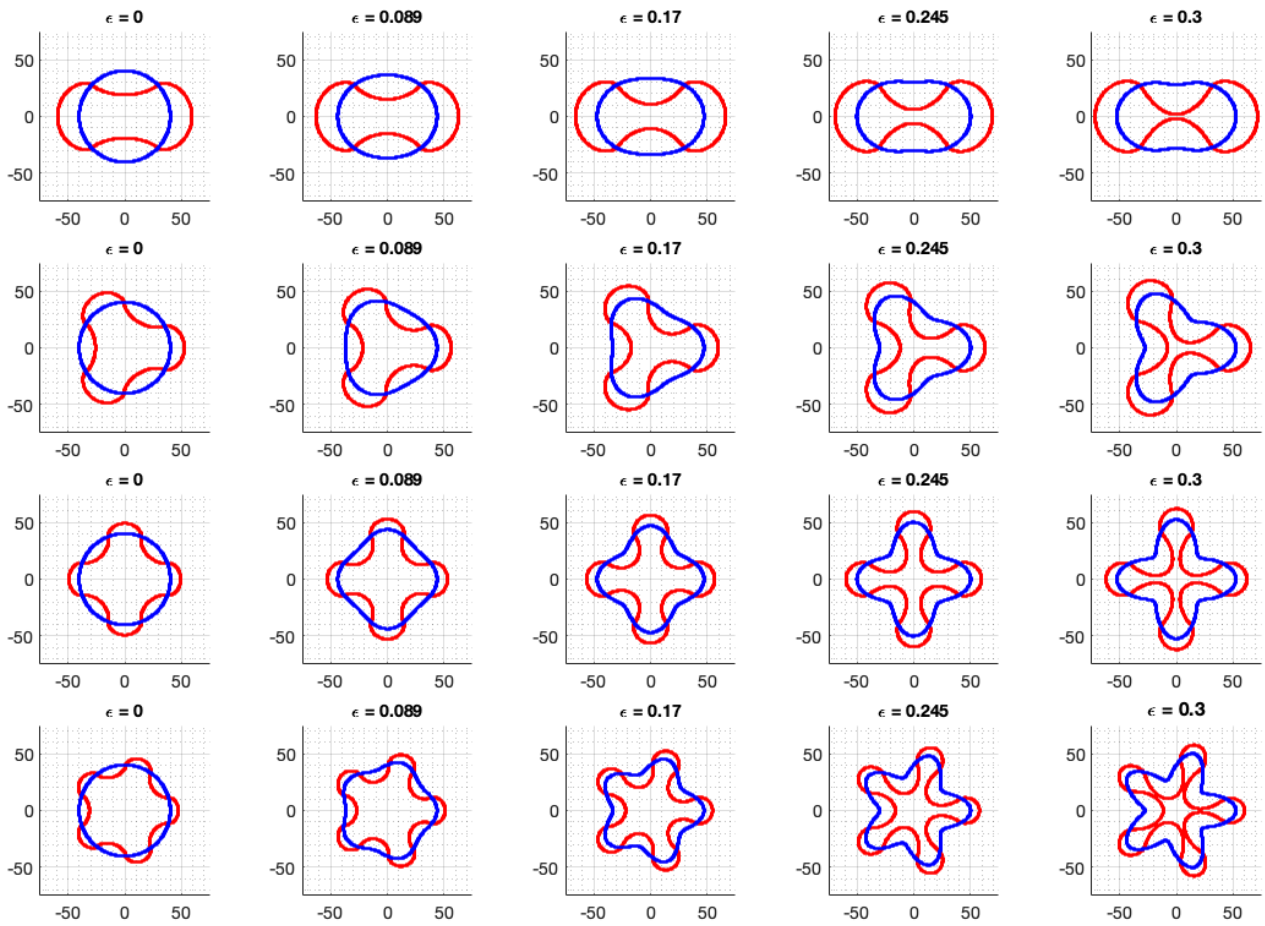

Figure 6. Roots rotor profiles with 2-5 lobes. Blue lines show the noncircular gear profiles, and red lines show the resulting rotor profiles from rolling a circle inside and outside the gears. Dimensions are in mm.

4.1. Air flow estimates

Each lobe of a rotor moves a pocket of air from the suction port to the discharge point. The pocket is formed from the volume of air trapped between the rotor and the housing. In one rotation, all lobes of both rotors deliver the air in their trapped pockets to the discharge port. For one rotation, the volume of air can be computed from the area of the minimum circle around the rotor minus the area of the rotor itself. The ratio of this air volume to the circle area is known as the *area utilization efficiency*, *area efficiency, or area utilization ratio*. The volume of air moved per revolution is the non-rotor area within the circle multiplied by the rotor height. The volume is then multiplied by the motor RPM to calculate the maximum output flow measured in CFM (cubic feet per minute)[1].

[1] CFM is a common way to specify the airflow of blowers and fans. In SI units, airflow may be specified in m^3/h (cubic meters per hour), CMM (cubic meters per minute), l/s (liters per second) or the standard SI unit of m^3/s (cubic meters per second). To covert the units, 1 CFM = ~0.00047 m^3/s. CFM is more commonly used for fans and HVAC because CFM values fall in a more convenient range than standard SI units. Other scaled SI units are also in a better range, but usage is not standardized and they scale the base SI units by powers of 60, making them less convenient for comparisons.

4.2. Gaps

Gaps between the rotors, as shown in Figure 6, reduce the flow because of the imperfect mismatch of the rotor profiles. Extra inter-rotor gaps may be added into the offset to allow for manufacturing tolerances. The volume of air in the rotor gaps is recirculated or returned to the exhaust port, reducing the net flow. The following tables use a version of the technique suggested by Ucer [14] to estimate the net flow. Air trapped in the gaps is treated like a separate port that delivers air from the discharge port to the suction port. This leakage flow is estimated by computing gap area as the average gap during a full rotation times the average radius at which the gap volume is delivered back to the input port. The average radius is just the average of the minimum and maximum rotor radii. This area is multiplied by the rotor height to get the volume and then multiplied by the RPM to get CFM loss. It is assumed that the entire gap air volume is delivered back to the suction port, reducing the flow by that amount.

4.3. Rotor comparisons

Table 1 shows the inputs and derived values for the profiles illustrated in Figure 6. The three input parameters that generate rotor profiles are the three left columns (*lobes*, *gear* ε, and *offset*). Other fixed input values (shaft spacing, rotor height, and motor RPM) are used for all calculations. The other columns show CFM loss, net CFM, and other derived parameters.

Table 1. Rotor parameters at 1000 RPM with rotor height 100 mm, shaft spacing 80.4 mm, and rotor-to-housing gap of 2 mm. *Offset* inputs are set to make the minimum rotor-rotor gaps close to 2 mm.

Lobes	Gear ε	Offset	Gaps min/avg	Lobes min/max	Housing diam	λ_g / λ_r	Area Efficiency	CFM loss	CFM net	CFM ratio
2	0	1	2.00 - 2.00	19.1 x 59.3	122.6	1.00/0.32	0.51	1.74	38.2	1
2	0.089	1.17	2.00 - 2.16	15.1 x 62.8	129.7	0.84/0.24	0.55	1.87	46.6	1.2
2	0.17	1.7	2.00 - 2.59	10.5 x 65.9	135.9	0.71/0.16	0.59	2.2	54.8	1.4
2	0.245	2.54	2.00 - 3.44	5.3 x 68.7	141.4	0.60/0.08	0.63	2.82	62.9	1.6
2	0.3	3.4	2.02 - 4.50	1.0 x 70.7	145.5	0.52/0.01	0.66	3.58	69.2	1.8
3	0	1	2.00 - 2.00	25.8 x 52.6	109.2	1.00/0.49	0.42	1.74	24.1	1
3	0.089	1.18	2.00 - 2.17	21.7 x 56.2	116.4	0.84/0.39	0.49	1.87	32.2	1.3
3	0.17	1.76	2.00 - 2.73	16.9 x 59.4	122.8	0.71/0.28	0.55	2.31	40.4	1.7
3	0.245	2.72	2.00 - 3.39	11.4 x 62.3	128.6	0.60/0.18	0.61	2.77	49.3	2.1
3	0.3	3.67	2.00 - 3.25	6.8 x 64.3	132.7	0.52/0.11	0.65	2.57	57.5	2.4
4	0	1	2.00 - 2.00	29.2 x 49.2	102.5	1.00/0.59	0.35	1.74	17.4	1
4	0.089	1.19	2.00 - 2.16	25.0 x 52.9	109.8	0.84/0.47	0.44	1.87	25.4	1.5
4	0.17	1.85	2.00 - 2.64	19.9 x 56.2	116.4	0.71/0.35	0.52	2.23	34.2	2
4	0.245	2.95	2.03 - 2.40	14.2 x 59.1	122.2	0.60/0.24	0.6	1.95	44.8	2.6
4	0.3	4	2.02 - 2.60	9.3 x 61.2	126.4	0.52/0.15	0.67	2.03	53.8	3.1
5	0	1	2.00 - 2.00	31.2 x 47.2	98.5	1.00/0.66	0.31	1.74	13.5	1
5	0.089	1.2	1.99 - 2.18	26.9 x 51.0	105.9	0.84/0.53	0.41	1.88	21.6	1.6
5	0.17	1.95	2.01 - 2.18	21.6 x 54.3	112.6	0.71/0.40	0.51	1.84	31.4	2.3
5	0.245	3.15	2.00 - 2.55	15.6 x 57.2	118.5	0.60/0.27	0.61	2.06	42.6	3.2
5	0.3	4.3	2.00 - 3.19	10.6 x 59.3	122.6	0.52/0.18	0.71	2.47	52.6	3.9

Note that the CFM loss increases much more slowly than the net CFM gain as ε increases. The highest flow is always at the most eccentric profile for a given number of lobes. When comparing two rows with the same number of lobes, the ratio of CFM improvement in the last column is greater than the value obtained by dividing the *Area Efficiencies*. The reason for the greater CFM increase is that for a fixed shaft spacing, the higher ε allows for a larger maximum lobe radius and larger diameter of the housing. Total volume increases as r^2 and this total area increase is multiplied by the *Area Efficiency* increase.

The lambda column shows λ_g, the ratio of minimum to maximum radius of the noncircular gear, along with λ_r, the minimum to maximum ratio of the rotor lobes. The ε values were chosen to show a range of rotor profiles with λ_g between 1 and .5.

In Table 1, the *offset* inputs were set to make the minimum gaps a generous 2 mm. This value is intentionally large to show that the losses are still small and that these profiles are good candidates for manufacturing processes with loose tolerances, such as 3D printers.

Table 2 shows the characteristics of rotors with 2-7 lobes, all with the same ε value. These use a much tighter *offset* to make the minimum gaps 0.1mm.

Table 2. Rotor parameters for Lobes 2-7 at 1000 RPM with rotor height 100 mm, shaft spacing 80.4 mm, and rotor to housing gap of 0.1 mm.

Lobes	Gear ε	Offset	Gaps min/avg	Lobes min x max	Housing diam	λ_g / λ_r	Area Efficiency	CFM loss	CFM net
2	0.245	1.59	0.10 - 1.54	6.3 x 69.7	139.5	0.60/0.09	0.61	1.3	64.7
3	0.245	1.77	0.10 - 1.49	12.4 x 63.2	126.7	0.60/0.20	0.58	1.25	50.6
4	0.245	1.99	0.10 - 0.48	15.1 x 60.1	120.3	0.60/0.25	0.58	0.4	45.6
5	0.245	2.2	0.10 - 0.66	16.6 x 58.2	116.6	0.60/0.28	0.58	0.54	42.9
6	0.245	2.41	0.10 - 0.72	17.4 x 56.9	114.1	0.60/0.31	0.59	0.6	41.9
7	0.245	2.6	0.10 - 0.34	17.9 x 56.0	112.3	0.60/0.32	0.61	0.28	42.2

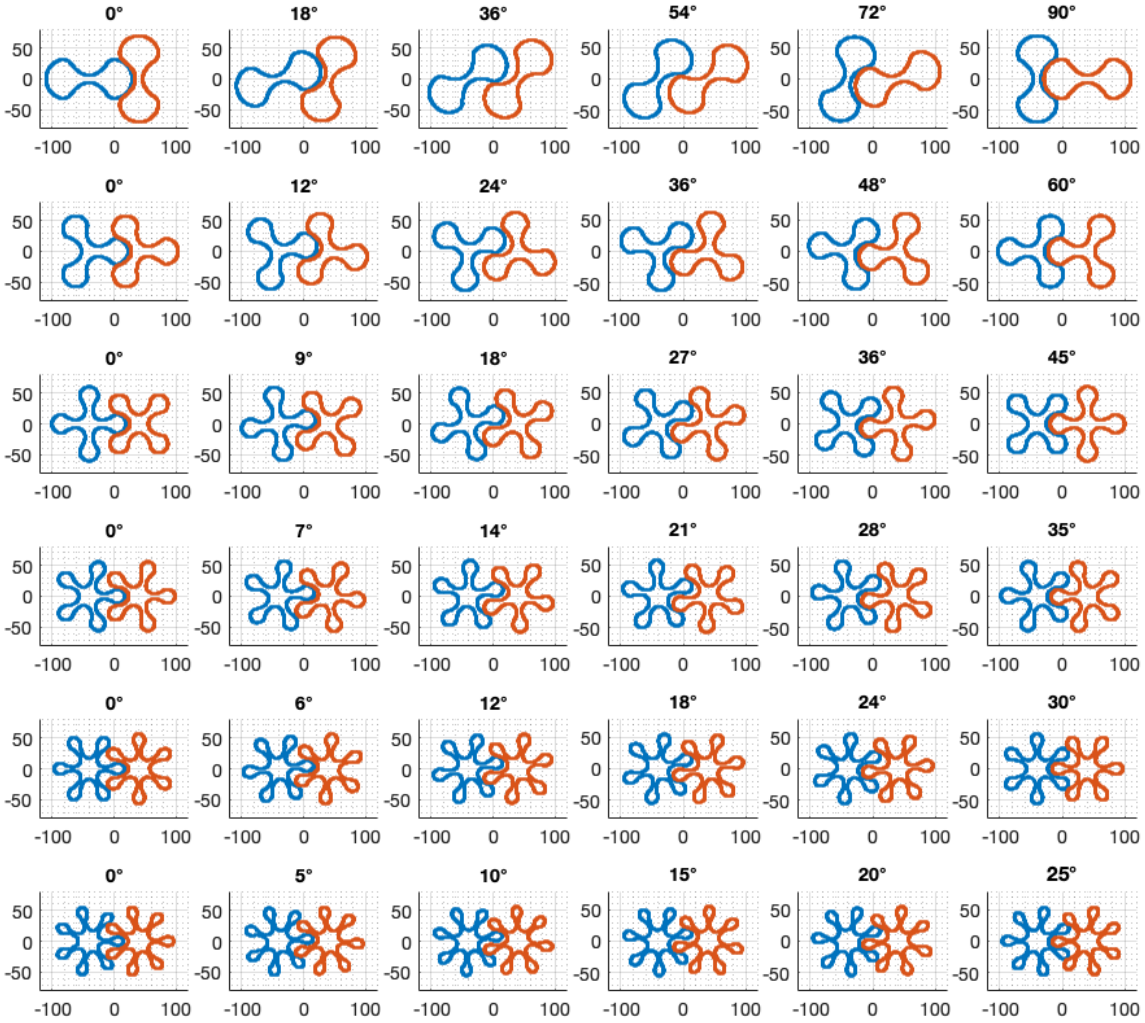

Figure 7. Meshing of rotors with 2-7 lobes with ε = .245 at six different rotations. Minimum gaps are 0.1 mm.

Figure 7 shows each of the six rotors of Table 2 at six different rotation angles. The CFM losses in these cases are due almost entirely to the carryover from the imperfect meshing of the profiles, but the losses are small compared to the large net CFM gained by these highly eccentric profiles. Examining these figures gives a visual reinforcement that the carryover volume is small compared to the volume of the air pockets delivered to the discharge port.

4.4. Helical rotors

The Roots profiles described in the equations and figures of this paper apply to either straight-lobe or helical rotors. Helical rotors introduce a twist along the length of the rotor and have been found to have more stable airflow, reduced eddy currents, and increased efficiency [15]. Yao also reported that three-lobe helical rotors have greater airflow, decreased exhaust pressure pulses, and lower noise [16]. Others have investigated rotor profiles for helical Roots blowers [17,18]

The helical twist angle, φ, must not introduce a channel for airflow directly between the input and output ports. When the housing has a semicircular wall for each rotor to contain the air pocket, the total angle of the air pocket (the lobe angle plus the twist angle) must be less than the containment angle of 180°. The air pocket angle is determined by the number of lobes, *N*, hence

$$\varphi <= \frac{\pi}{2} - 2\pi/N \tag{9}$$

Table 3. Allowable helical twist angles.

Lobes	Air Pocket angle	Maximum φ	Lobe twists
2	180°	0°	0
3	120°	60°	0.5
4	90°	90°	1
5	72°	108	1.5
6	60°	120°	2
7	51°	129°	2.5

Table 3 shows the maximum allowable twist angle for Roots rotors with 2-7 lobes, although these angles can be increased slightly by extending the housing around each rotor to > 180°. The last column measures the maximum twist angle by the number of lobe twists. A twist of 1 means that the top and bottom of the rotor have the end of the lobe directly above the start of the lobe, but the bottom lobe is twisted on the way to the other end. When the twist = 1, the airflow should be the same at every rotation angle because every combination of lobe angles is found somewhere between the ends of the rotor. The 3-lobe helical rotors can only be twisted half of one lobe, but those with 4 or more lobes can have a full twist.

If the output port is restricted to less than the full height of the rotor, it is possible to have helical twists greater than that shown in Table 3. The output restriction also causes a compression of the air at discharge which is beneficial in some applications. Zhao has proposed such a structure for an air

compressor for a hydrogen fuel cell vehicle [19]. The rotor profiles presented in this paper could also apply to these applications.

4.5. Fabrication

The following technique is used to fabricate rotors based on equations 6-8: First, a program is written in Matlab, Python or another language, to implement the equations plus the offsets. The code also exports the X and Y coordinates of the profile into a csv file with sufficient points to produce a smooth curve. In practice, a range from 180 to 1001 points have been used successfully. Next, a 3D CAD program such as Autodesk Fusion uses a script such as ImportSplineCSV to convert the csv file points to a closed spline shape. The shape is then extruded with a twist along the path of a construction line running through the shaft center. The extruded shape is then modified with any other mounting holes or structures, and exported as a STEP file or mesh file. The 3D slicer then imports the STEP or mesh file, slices it, and prints it. Rotors may be 3D-printed with zero infill to make the rotors hollow because hollow rotors are faster to print, consume less material, and avoid uneven fill material which could affect their balance. When the rotors are helical, separate models for left and right twists must be produced and printed. Figure 8 shows the results of a 3D print for a 5-lobe rotor with a helix angle of 72° which is one full lobe twist.

Figure 8. 3D-printed 5-lobe rotors with helix angle 72° and ε = 0.3

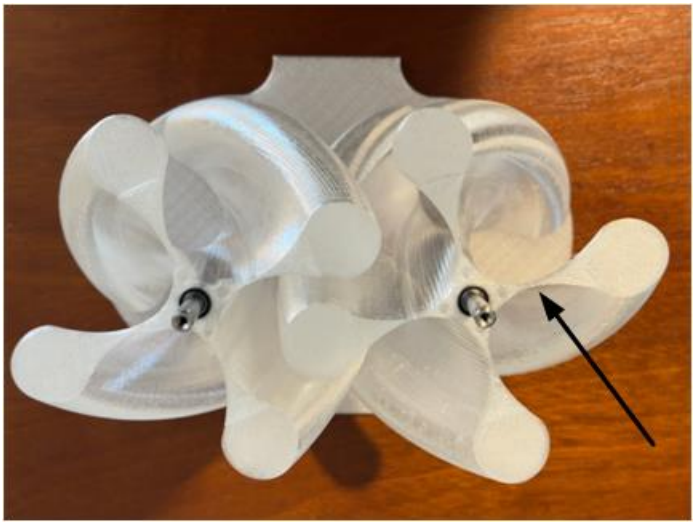

Figure 9. 3D-printed 4-lobe rotors with helix angle 90° and ε = 0.3

Figure 9 shows a 4-lobe helical rotor with a minimum gap of 7 mm and a full lobe twist of 90°. For this rotor, the large minimum gap makes the minimum lobe width just 1.6 mm, as indicated by the arrow. Although this might seem weak, the lobe is still held to the shaft by the total cross-section of 1.6 mm times the path length of the lobe height. For a straight-lobe rotor 100 mm high, each lobe would be attached by a cross-section of 160 mm^2. If the lobe is printed with PETG, the tensile strength in the YZ direction is approximately 44 MPa [20]. The force to break off a lobe is then 16,000 N (3597 lbf). The helical rotor is even stronger because the path length of the helix is longer. With either straight-lobe or helical rotors, the material strength far exceeds the centrifugal forces from the rotation. In other cases, if analysis shows that rotor strength needs to be increased, the family of profiles in this paper makes it easy to do so. As shown in Figure 6 and Table 1, a small decrease in eccentricity results in a large increase in the lobe width in order to increase strength at the cost of a small decrease in airflow.

4.6. Comparison with other profiles

It can be difficult to compare Roots profiles presented in different papers because they present results in different ways. Some papers omit area efficiency calculations, and many do not specify rotor dimensions. However, many papers include enough information to determine the ratio of the minimum to maximum diameter of the lobes, as shown in Table 4.

Some papers give this ratio (or its inverse) directly, some give the rotor dimensions, and some give the shaft spacing and chamber radius (~= maximum rotor radius) which allows derivation of the minimum radius. Half of the shaft spacing is the pitch radius. Subtracting pitch radius from the chamber radius gives the delta to be added or subtracted from the pitch radius to determine the maximum and minimum rotor radii.

Table 4. Comparison of width to length ratios of lobes from recent papers on improved Roots profiles.

Reference	Rotor type	Lobes	SS	Max R	Min R	λ_r
Shujun 2011 [21]	Traditional involute	3				0.683
	Improved involute	3				0.680
Wu 2018 [3]	IVEC (Involute and Variable-Extended Cycloids)	2	80	63	17	0.270
		3	66	44	22	0.500
Xing 2021 [22]	Four curves plus involute	3	280	209.75	70.25	0.335
		6	280	185	95	0.514
Zhao 2022 [19]	Helical 160 deg wrap	4	43.36	32.05	11.31	0.353
Zhou 2023 [23]	Four arcs, epicycloid, and involute	3				0.680

The last column shows λ_r, the ratio of minimum to maximum radius of the rotor. Smaller numbers indicate lobes that are more eccentric and that devote more area to air pockets instead of the rotor itself. The smallest number from these recent papers is 0.270, meaning that the lobe length is 3.7 times its width. Comparing these values with those from Tables 1 and 2, the new profiles clearly have much larger areas devoted to air pockets and hence will have greater air flow. In Table 1, with $\varepsilon = 0.3$, λ_r ranges from .01 to .18, indicating length-to-width ratios of 5.6:1 to 100:1. Figure 10 below, from one of the references, shows rotor profiles that clearly have smaller air pockets than the new profiles shown in Figure 6.

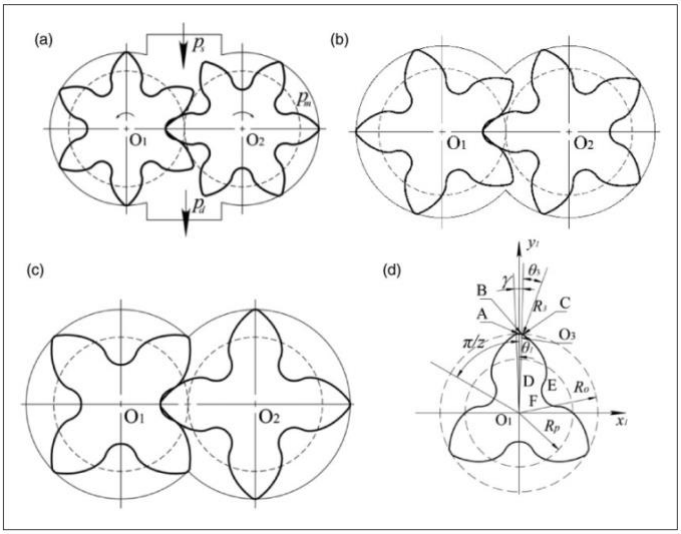

Figure 10. Prior Roots profiles from Figure 5 of Xing 2021 [22].

5. Conclusions

This paper has described and analyzed a new family of high-flow Roots profiles. It is hoped that the simplified equations will help engineers implement these profiles more easily than those based

on more complex mathematical derivations. The equations simply describe profiles based on a circle rolling around a noncircular gear, and the simplifications stem from the lessons learned in the analysis of the coin rotation paradox. The equations take advantage of previous work in noncircular gear theory but advance that to produce an equation that produces a range of identical noncircular gears with any number of lobes. Interferences in the resulting profiles are eliminated by offsetting the profiles. The resulting profiles are much more eccentric and higher-flow than traditional Roots profiles. Estimates of the flow rates show that the small amount of carryover is more than overcome by the greater flow rates of the new profiles. The profiles can be built as either straight-lobe or helical rotors.

Roots blowers with relaxed manufacturing tolerances, high air movement, and low noise may see more applications in home devices such as air filters, range hoods, bathroom vents, hair dryers, and leaf blowers, which are currently served by squirrel cage blowers or ducted fans. The profiles described in this paper may be a step toward these wider applications.

Acknowledgment

The author thanks Doug Jewett, Chuck McManis, Joe West, Philip Rakity, and Simon Quellen Field for helpful technical discussions and assistance in preparing this document.

References

1. P.H Roots, "Rotary blower," U.S. Patent 2369 (1860).
2. W.L. Palmer and I.W. Knox, "Improvement in rotary pressure-blowers, " U.S. Patent 166,296, (1875).
3. Wu, Yu-Ren, and Van-The Tran. "Generation method for a novel Roots rotor profile to improve performance of dry multi-stage vacuum pumps." *Mechanism and Machine Theory* 128 (2018): 475-491.
4. Ucer, S., and I. Celik. "Analysis of flow through roots blower systems." (1980).
5. Zhou, Shuangmei, et al. "The effects of design parameters on performance of a novel roots profile." *International Journal of Hydrogen Energy* 48.6 (2023): 2368-2384.
6. Tien, Tran Ngoc, and Nguyen Hong Thai. "A novel design of the roots blower." *Vietnam Journal of Science and Technology* 57.2 (2019): 249-260.
7. Tong, Shih-Hsi, and Daniel CH Yang. "Generation of identical noncircular pitch curves." (1998): 337-341.
8. Litvin, Faydor L., et al. "Design and investigation of gear drives with non-circular gears applied for speed variation and generation of functions." *Computer methods in applied mechanics and engineering* 197.45-48 (2008): 3783-3802.
9. Bair, Biing-Wen, et al. "Tooth profile generation and analysis of oval gears with circular-arc teeth." *Mechanism and machine theory* 44.6 (2009): 1306-1317.
10. Tong, Shih-Hsi, and Daniel CH Yang. "Generation of identical noncircular pitch curves." (1998): 337-341.
11. Tien, Tran Ngoc, and Nguyen Hong Thai. "A novel design of the roots blower." *Vietnam Journal of Science and Technology* 57.2 (2019): 249-260.
12. Zarębski, Igor, and Tadeusz Sałaciński. "Designing of non-circular gears." *Archive of Mechanical Engineering* (2008): 275-292.
13. Harris, Michael J. "The SAT Problem That Everybody Got Wrong." *Scientific American*, 20 June 2023.
14. Ucer, S., and I. Celik. "Analysis of flow through roots blower systems." (1980).

15. Tran, Ngoc-Tien, and Duc-Minh Nguyen. "Analysis of flow characteristics of cylindrical and helical type multi-lobe roots blower." *EUREKA: Physics and Engineering* 1 (2023): 67-75.
16. Yao, Ligang, et al. "Geometric analysis and tooth profiling of a three-lobe helical rotor of the Roots blower." *Journal of Materials Processing Technology* 170.1-2 (2005): 259-267.
17. Xing, Linfen, et al. "Analysis and development of a roots-type air compressor with fixed internal compression for fuel cell system." *Proceedings of the Institution of Mechanical Engineers, Part A: Journal of Power and Energy* 236.1 (2022): 51-60.
18. Li Tran, Ngoc-Tien, and Duc-Minh Nguyen. "Analysis of flow characteristics of cylindrical and helical type multi-lobe roots blower." *EUREKA: Physics and Engineering* 1 (2023): 67-75., Dantong, et al. "Development and analysis of novel six-lobe helical rotors for hydrogen fuel cell vehicle roots blowers." *International Journal of Hydrogen Energy* 46.59 (2021): 30479-30493.
19. Zhao, Bin, et al. "Investigation of 3D transient flow and discharge pressure pulsation of helical roots air compressor for hydrogen fuel cell vehicle." *Proceedings of the Institution of Mechanical Engineers, Part C: Journal of Mechanical Engineering Science* 236.23 (2022): 11231-11239.
20. Ultimaker PETG Technical Datasheet, https://um-support-files.ultimaker.com/materials/2.85mm/tds/PETG/Ultimaker-PETG-TDS-v1.00.pdf
21. Shujun, Wang, et al. "The improvement study of involutes profile type rotor profile in Roots vacuum pump." 2011 International Conference on New Technology of Agricultural. IEEE, 2011.
22. Xing, Linfen, et al. "Performance improvement of a large capacity Roots blower based on profile modification." *Proceedings of the Institution of Mechanical Engineers, Part C: Journal of Mechanical Engineering Science* 235.13 (2021): 2386-2394.
23. Zhou, Shuangmei, et al. "The effects of design parameters on performance of a novel roots profile." *International Journal of Hydrogen Energy* 48.6 (2023): 2368-2384.